Electronic Supplementary Material (ESI) for Nanoscale.

Supporting Information: *In situ* study of the precursor conversion reactions during solventless thermolysis of Co_9S_8, Ni_3S_2, Co and Ni nanowires

John A. Scott,* Alexander Angeloski, Igor Aharonovich, Charlene J. Lobo, Andrew McDonagh* and Milos Toth *

School of Mathematical and Physical Sciences, University of Technology Sydney

E-mail: Andrew.Mcdonagh@uts.edu.au
E-mail: Milos.Toth@uts.edu.au

*To whom correspondence should be addressed

Experimental

Precursor solutions for the growth of Co_9S_8 and Co nanowires: Solutions suitable for thermolysis were prepared by dissolving a mixture of cobalt(II) acetate tetrahydrate and L-cysteine in millipore water (18.4 MΩ cm^{-1}). The cysteine mass was kept standard to achieve 9.0 ± 0.5 mM solutions whilst appropriate amounts of cobalt(II) acetate were added to obtain solutions with Co^{II}:Cys mole ratios ranging from 0.9 to 9.7. The Co^{II}:Cys mole ratio solutions with the mass of cobalt(II) and cysteine are shown in Table S1.

Precursor solutions for the growth of Ni_3S_2 and Ni nanowires: Solutions suitable for thermolysis were prepared by dissolving a mixture of nickel(II) tetrahydrate and L-cysteine in millipore water (18.4 MΩ cm^{-1}). The cysteine mass was kept standard to achieve 9.0 ± 0.5 mM solutions whilst appropriate amounts of nickel(II) acetate were added to obtain solutions with Ni^{II}:Cys mole ratios ranging from 1.0 to 4.9. The Ni^{II}:Cys mole ratio solutions with the mass of nickel(II) acetate and cysteine are shown in Table S2. To achieve Ni_3S_2 nanowire growth a 5 mL aliquot was taken from the 1.0 Ni^{II}:Cys mole ratio solution. To this approximately 3 mL of hydrogen peroxide solution (30 % w/w in water) was added. The solution appeared to turn clear.

Precursor characterization: UV-visible (UV-vis) absorbance characterization of the Cobalt(III) bis-cysteinate complex was done on both stock solutions prepared by mixing the reagents as described above and also by isolating the Cobalt(III) bis-cysteinate complex through filtration of the crude reaction mixture. The crude reaction mixture was clarified by filtration through a 0.45 µm syringe filter, and the resultant filtrate was collected. Purification of the crude filtrate was achieved by addition of chloroform, followed by a sufficient volume of methanol to achieve a uniform solution. Upon cooling, a dark green material was precipitated and collected by vacuum filtration, resulting in a pale pink filtrate and an oily green-brown filter cake. The latter was repeatedly triturated using cold methanol and then dried in vacuum. A similar process was performed for the isolation of the nickel(II) bis-cysteinate precursor.

Degassed aqueous solutions of cobalt acetate (40 mM) and cysteine (8.6 mM) were prepared by dissolving into separate already degassed (0.1% acetic acid v/v) aqueous solutions. Degassing was done by purging N_2 through each solution for 30 minutes before adding cysteine and cobalt(II) acetate to the respective solutions. Degassing was continued for a further 10 minutes before the cobalt(II) acetate solution was mixed into the cysteine solution whilst stirring. Upon air exposure, the resulting orange solutions gradually changed to a dark brown colour (Figure S14).

Nanowire growth: 30 µL of the precursor solution was dropcast onto clean Si substrates (with a thermal oxide) held at $100^{o}C$. Following solvent evaporation, the substrate was loaded into the vacuum chamber, pumped to high vacuum (1×10^{-7} mbar) and heated to the desired growth temperature. The temperature was measured using a single thermocouple placed directly onto a mock Si substrate located adjacent to the growth substrate (on the heater). The typical heating rate was 3 - 4^{o}C/sec. Annealing temperature for Co_9S_8/Co nanowire growth was 590 ± 20^{o}C, the total time at this temperature was 1 hour. For Ni_3S_2 nanowire growth the annealing conditions were 415 ± 10^{o}C for 5 hours. The substrates were cooled under high vacuum before removal for characterisation.

Mass spectrometry, UV-Vis and FTIR spectroscopy: High resolution mass spectrometry (HRMS) was performed using an Agilent 6510 Q-TOF with a mobile phase of 70% acetonitrile, 30% water and a flow rate of 0.5 mL/minute. FTIR spectra were acquired using a Nicolet 6700 FTIR spectrometer fitted with a diamond smart iTX ATR accessory. Each spectrum was collected using 64 scans, with a resolution of 2 cm^{-1} over the range of 5000 - 600 cm^{-1}. UV-Vis spectra of aqueous solutions were acquired using a Cary 60 spectrometer from 190 to 800 nm at 0.5 nm resolution. HRMS (M+) for $[CoC_6H_{12}N_2O_4S_2]^+$ Calculated: 298.9565; Observed: 298.9580.

Thermogravimetric analysis and gas chromatography (TGA-GC-MS) were performed using a Netzsch STA 449 F5 Jupiter thermal analyser coupled with a heated transfer line to an Agilent 7890/5977 GC/MS. Samples were placed in a 90 µL alumina crucible, and experiments were conducted using an atmosphere of helium (100 mL min^{-1}) and a heating rate of 3 °C min^{-1} from 30 to 900 °C. A 150 µL aliquot of furnace gas was subjected to a 1:5 dilution with helium, and a small quantity injected every 8 minutes through an Agilent HP-5MS column, with separation achieved using a temperature ramp from 50 to 200 °C with a heating rate of 20 °C min^{-1}.

SEM, EDS, XRD, HRTEM and SAED characterization: The growth products were imaged using a Zeiss Supra 55VP scanning electron microscope (SEM), using an Oxford Instruments INCA X-Sight 7558 for energy dispersive X-ray spectroscopy (EDX) microanalysis. Transmission electron microscope (TEM) and high resolution TEM (HRTEM) imaging and selected area electron diffraction were performed on a FEI Tecnai T20 TWIN microscope (LaB6) operating under an accelerating voltage of 200 kV. Selected are electron diffraction (SAED) characterisation of a gold standard was used for calibration of plane spacing measurements. A Bruker Discover D8 Powder X-ray diffractometer with Cu Kα (λ = 1.54060 Å) was used to acquire diffractograms. Nanowire growth substrates were characterised using grazing-angle incidence X-ray diffraction, the scanning range (2θ) was 20-80^{o} with a step size of 0.02^{o}. The TGA-GC-MS powder residue X-ray diffraction data was acquired using a coupled scan. For the Co^{III} bis-cysteinate residue the scan range was 14-70^{o} and Ni^{II} bis-cysteinate 20-60, step sizes were 0.02^{o} for both. Characterisation of nanowires during growth was performed using a customized Sirion field-emission gun SEM. A homemade heating stage was used to heat the sample to growth temperature (540 ^{o}C) under high vacuum (9 x 10^{-6} mbar). Temperature was measured by a thermocouple clipped to the heating stage.

S1 Heating rate

The recorded heating rate and annealing temperature profiles for Co_9S_8, Co, Ni_3S_2 and Ni nanowire growths resulting from the starting 0.9 and 4.9 Co^{II}:Cys and 1.0, 3.9 and 4.9 Ni^{II}:Cys mole ratio solutions is shown in Figure S1.

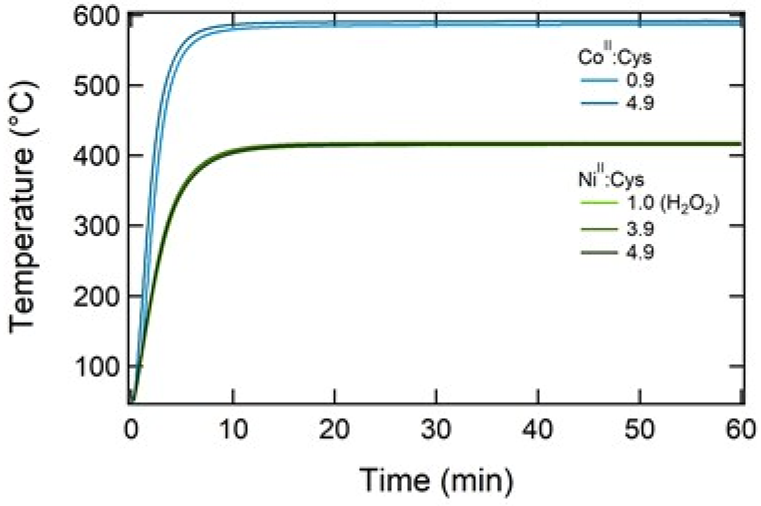

Figure S1. The heating rate and annealing profile for nanowire growths.

S2 Co_9S_8 and Co nanowire precursor solutions with diameter and length distributions

Table S1 shows the precursor solutions with the Co^{II}:Cys mole ratios: 0.9, 4.9 and 9.7 and the respective pH and starting reagent masses (cobalt(II) acetate and cysteine). The Co_9S_8 nanowire diameter and length distribution is shown in Figure S2 and S3 respectively. The cobalt nanowire diameter and length distribution is shown in the Figures S4 and S5 respectively.

Table S1: Precursor solutions for Co_9S_8 and Co nanowire growth.

Co^{II}:Cys		Mass (mg)	
Mole Ratio	pH	Co^{II} acetate	Cysteine
0.9	4.8	100	50
4.9	5.4	500	50
9.7	5.7	1000	50

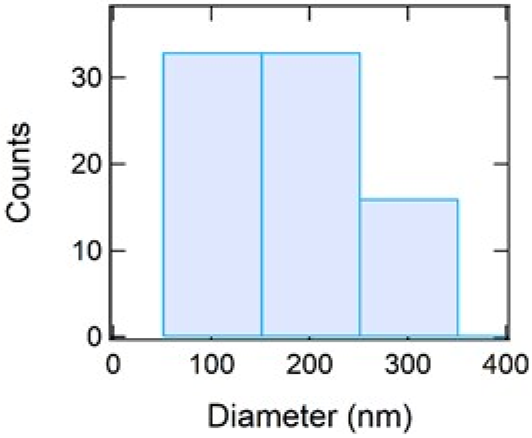

Figure S2. Histogram showing Co_9S_8 nanowire diameter distribution.

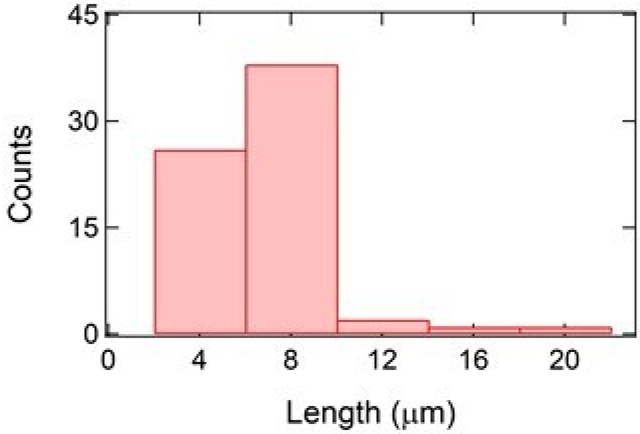

Figure S3. Histogram showing Co_9S_8 nanowire length distribution.

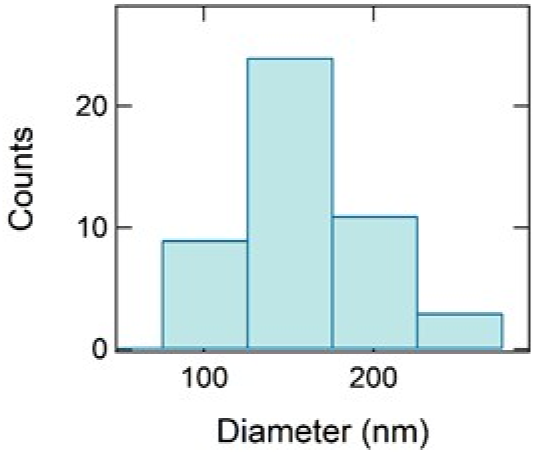

Figure S4. Histogram showing Co nanowire diameter distribution.

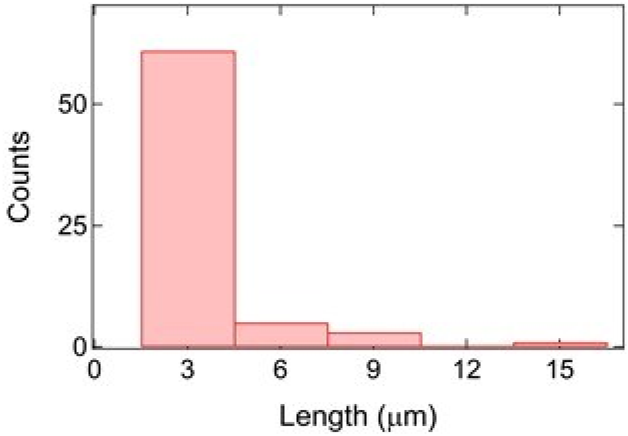

Figure S5. Histogram showing Co nanowire length distribution.

S3 Determination of nanowire growth direction

Nanowire growth direction can be determined by several different techniques using TEM and SAED characterization.[1] By aligning the nanowire growth direction perpendicular to the electron beam the sharp edge of the nanowire induces a streaking in the diffraction intensity spots along a direction perpendicular to the nanowire growth axis.[1] We confirm this result by comparing the SAED pattern with the shadow image of the nanowire recorded in diffraction mode (under identical camera lengths). Figure S6a shows the recorded shadow image captured in diffraction mode of a cobalt sulfide nanowire (diameter = 70 nm) and Figure S6b shows the corresponding SAED pattern of the nanowire. The nanowire growth axis, as highlighted by the red arrow, was determined by the streaking effect and confirmed by comparing with the shadow image. Identical characterisation was done on a second nanowire and a different zone axis ([-112]) as shown in Figure S6c and d. The nanowire growth axis is again shown to be perpendicular to the elongation in the diffraction intensity spots, justifying the technique to deduce the growth axis.

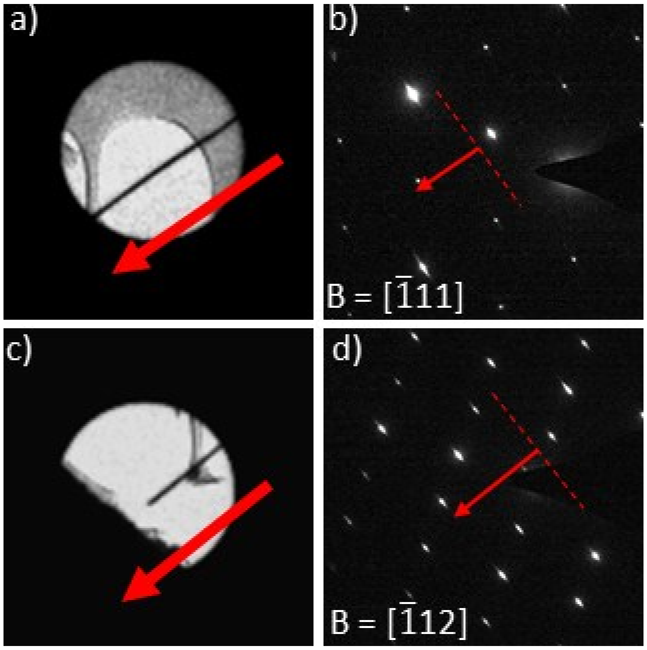

Figure S6. a) Shadow image of a Co_9S_8 nanowire captured in diffraction mode. b) SAED pattern from nanowire in a) captured with the same camera length. c) Shadow image of a second Co_9S_8 nanowire captured in diffraction mode with the corresponding d) SAED pattern.

S4 Co_9S_8 nanowire characterisation

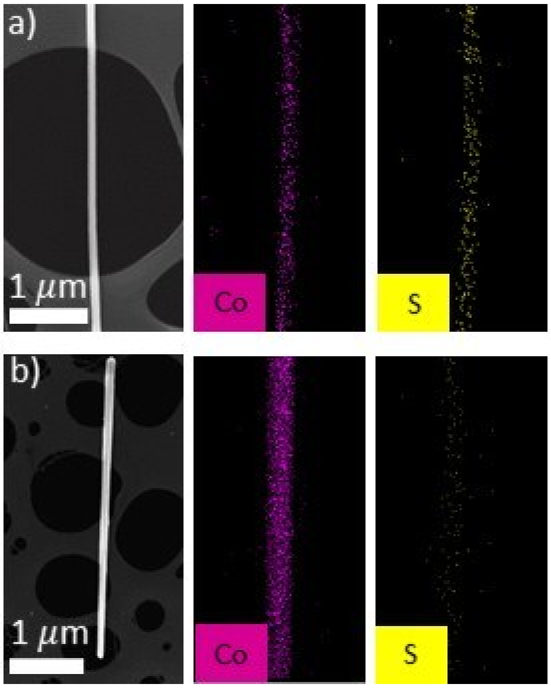

Figure S7. a) SEM image of a Co_9S_8 nanowire on a Cu TEM grid with a holey carbon membrane with cobalt and sulfur elemental maps using EDS of the nanowire. b) SEM image with cobalt and sulfur elemental maps of a Co nanowire. e) TEM image of a 80 nm diameter nanowire with f) SAED resolved along the [001] zone axis.

Figure S7 shows SEM and EDS characterisation of isolated Co_9S_8 and Co nanowires, obtained from starting 0.9 and 4.9 (Co^{II}:Cys) mole ratio solutions, respectively. An isolated Co_9S_8 nanowire transferred onto a Cu TEM grid with a supportive carbon membrane is shown in the SEM image in Figure S7a. The TEM grid was housed on an elevated Al TEM grid holder sitting on the SEM stage to minimize background contributions to the X-ray signal. Compositional analysis by EDS confirmed the presence of both Co and S in the 100 nm diameter nanowire (Figure S7a).

SEM characterization of a 100 nm diameter Co nanowire, along with EDS elemental mapping of Co and S is shown in Figure S7d. The S signal shows much lower counts (compared with the Co_9S_8 nanowire) and is attributed to a capping layer surrounding the Co nanowire.

S5 Ni_3S_2 and Ni nanowire precursor solutions and diameter distributions

Table S2 shows the precursor solutions with the Ni^{II}:Cys mole ratios: 1.0, 3.9 and 4.9 and the respective pH and starting nickel(II) acetate and cysteine masses. The diameter distributions for the resulting Ni_3S_2 and Ni nanowire growths are shown in Figure S8 and S9 (respectively).

Table S2: Precursor solutions for Ni and Ni_3S_2 nanowire growth.

Ni^{II}:Cys		Mass (mg)	
Mole Ratio	pH	Ni^{II} acetate	Cysteine
1.0	4.5	100	50
3.9	5.0	400	50
4.9	5.0	500	50

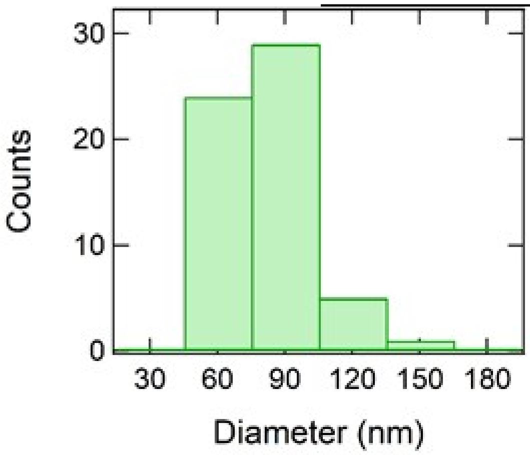

Figure S8. Histogram showing Ni_3S_2 nanowire diameter distribution.

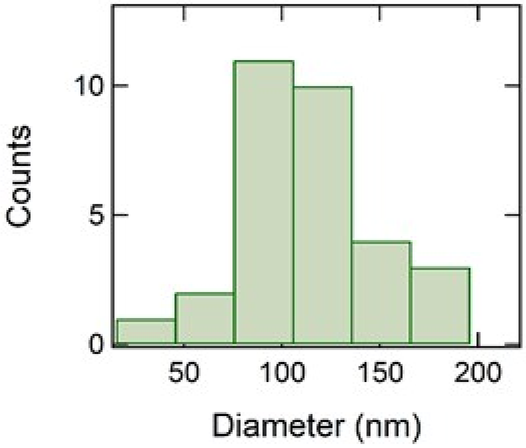

Figure S9. Histogram showing Ni diameter distribution.

S6 Ni$_3$S$_2$ and Ni nanowire characterisation

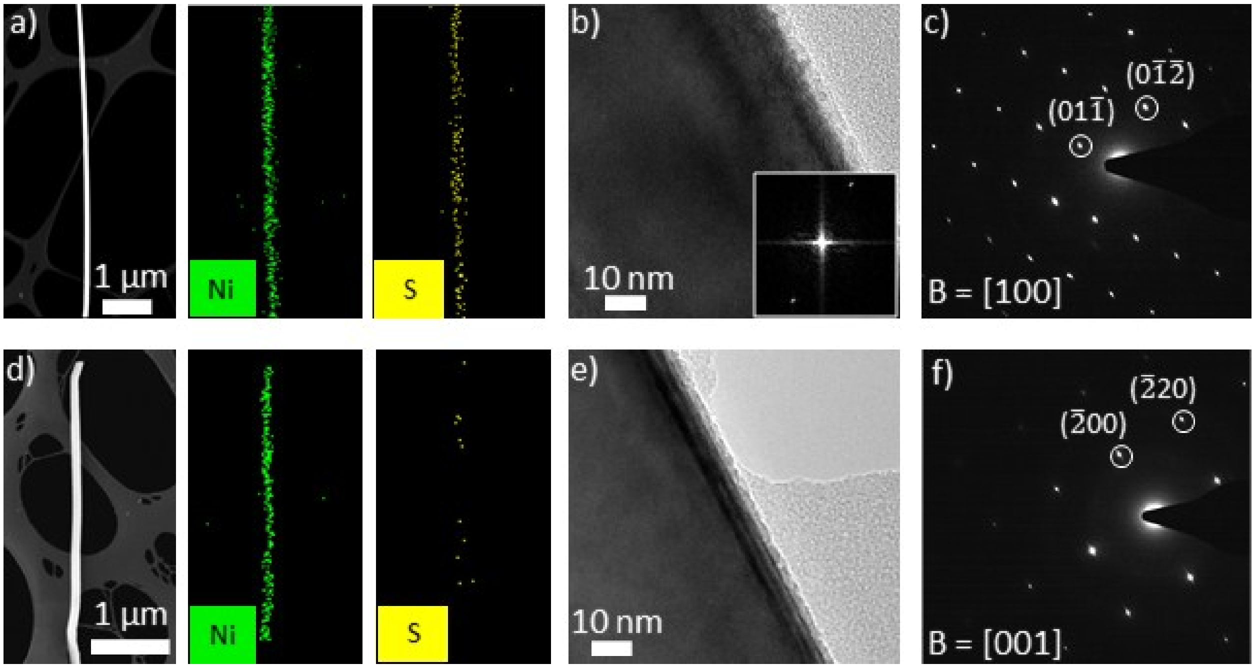

Figure S10. a) SEM image of a Ni$_3$S$_2$ nanowire on a Cu TEM grid with a holey carbon membrane with nickel and sulfur elemental maps using EDS of the nanowire. b) Lattice fringe resolved TEM image of a 80 nm Ni$_3$S$_2$ nanowire with FFT (inset). c) SAED pattern from nanowire in b) resolved along the [100] zone axis. d) SEM image of an isolated Ni nanowire (100 nm in diameter) with Ni and S elemental maps shown in green and yellow (respectively). e) TEM image of a 110 nm diameter nanowire with f) SAED resolved along the [001] zone axis.

An SEM image of a Ni$_3$S$_2$ nanowire transferred onto a Cu TEM grid with a holey carbon membrane is shown in Figure S10a. The elemental EDS maps confirm approximately equivalent intensities for both Ni and S (shown in green and yellow respectively). Figure S10b shows a TEM image of an isolated Ni$_3$S$_2$ nanowire approximately 80 nm in diameter. The lattice fringe resolved image shows the nanowire to be crystalline with an amorphous capping layer. A FFT of the nanowire lattice is shown in the inset. The SAED pattern can be indexed as the rhombohedral R32 space group using the Ni$_3$S$_2$ parameters and shows the nanowire to be single-crystal (Figure S10c). The zone axis is [100], and the {110} plane spacing was measured to be 3.95 Å which is in good agreement with theoretical values for rhombohedral Ni$_3$S$_2$ (4.081 Å). A SEM image and elemental

EDS maps for Ni and S are shown in Figure S10d for an isolated 110 nm diameter Ni nanowire transferred to a holey carbon grid. HRTEM (Figure S10e) and SAED (Figure S10f) show the nanowire to be single crystal fcc cubic; the lattice spacings of the {200} planes (3.35 Å) were in agreement with fcc Ni (3.524 Å).

S7 UV-vis and FTIR spectroscopy and optical characterisation of the precursor solutions.

UV-vis absorbance spectra of the [$Co^{III}Cys_2(H_2O)_2$] (Figure S11a) and both the 0.9 and 4.9 Co^{II}:Cys precursor solutions (Figure S12a) exhibit a low intensity band at 579 nm ($\epsilon = 406\ M^{-1}cm^{-1}$) and three medium intensity bands at 440 ($\epsilon = 1302\ M^{-1}cm^{-1}$), 350 ($\epsilon = 3476\ M^{-1}cm^{-1}$) and 280 nm ($\epsilon = 4600\ M^{-1}cm^{-1}$). The presence of four bands is characteristic of six coordinate Co^{III} complexes in an octahedral sphere which give rise to the spin allowed ($^1A_{1g} \rightarrow {}^1T_{2g}$ and $^1A_{1g} \rightarrow {}^1T_{1g}$) and two spin forbidden ($^1A_{1g} \rightarrow {}^3T_{2g}$ and $^1A_{1g} \rightarrow {}^3T_{1g}$) transitions.[2] The multiple band at 515 nm due to the $^4T_{1g} \rightarrow {}^4T_{1g}(P)$ transition from $Co(H_2O)_6{}^{2+}$ in the cobalt(II) acetate solution is not observed as it is of low intensity ($\varepsilon = 4.6\ M^{-1}cm^{-1}$) and obscured by the precursor complex. The identical absorbance maximum in each of the precursor solutions indicates that the inner coordination sphere of the cobalt complex remains unchanged with varying Co:Cys ratios.

UV-vis absorbance spectra for the 1.0, 3.9 and 4.9 Ni^{II}:Cys precursor solutions (Figure S12b) show three broad *d-d* absorption bands at 680 nm, 460 and 375 nm. These bands are assigned to the $^1A_{1g} \rightarrow {}^1A_{2g}$, $^1A_{1g} \rightarrow {}^1B_{1g}$ and $^1A_{1g} \rightarrow {}^1E_g$ transitions respectively.[3-6] These three bands are characteristic of square planar d^8 nickel(II) complexes, and in agreement with the solid state structure of $Ni^{II}Cys_2$.[7] A band at 270 nm is attributed to intraligand transitions. The nickel(II) acetate bands expected at 395 ($\varepsilon = 5.0\ M^{-1}cm^{-1}$), and 724 nm ($\varepsilon = 2.0\ M^{-1}cm^{-1}$) due to the $^3A_{2g} \rightarrow {}^3T_{1g}(P)$ and $^3A_{2g} \rightarrow {}^3T_{1g}$ transition from $Ni(H_2O)_6^{2+}$ were not observed in the nanowire precursor solutions due to their low intensity.

The FTIR spectrum of the isolated cobalt-cysteine product (Figure S13) shows bands at 800 (CO_2 bend), 1046 (NH_2 rock), 1314 (CH_2 wag), 1390 (CO_2 sym.), 1417 cm^{-1} (CH_2 bend), 1535 (NH_2 bend), 1600 (CO_2 str. asym.) and 3204 cm^{-1} (OH stretch) which are in agreement with reported values for coordinated cysteine in Co^{III} bis-cysteinate.[8] The presence of antisymmetric

(1600 cm^{-1}) and symmetric (1390 cm^{-1}) CO_2 associated vibrations, and similarity of -CO_2 frequencies to un-coordinated cysteine indicates that the carboxylic moiety is not involved in coordination to the cobalt metal centre.[8]

The FTIR spectrum of the isolated nickel-cysteine product (Figure S13) shows bands at 801 (CO_2 bend), 1065 (NH_2 rock), 1393 (CO_2 sym), 1552 (NH_2 bend), 1583 (CO_2 str. asym) and 3274 cm^{-1} (OH stretch), similar to those of the Co^{III} bis-cysteinate spectrum described above.

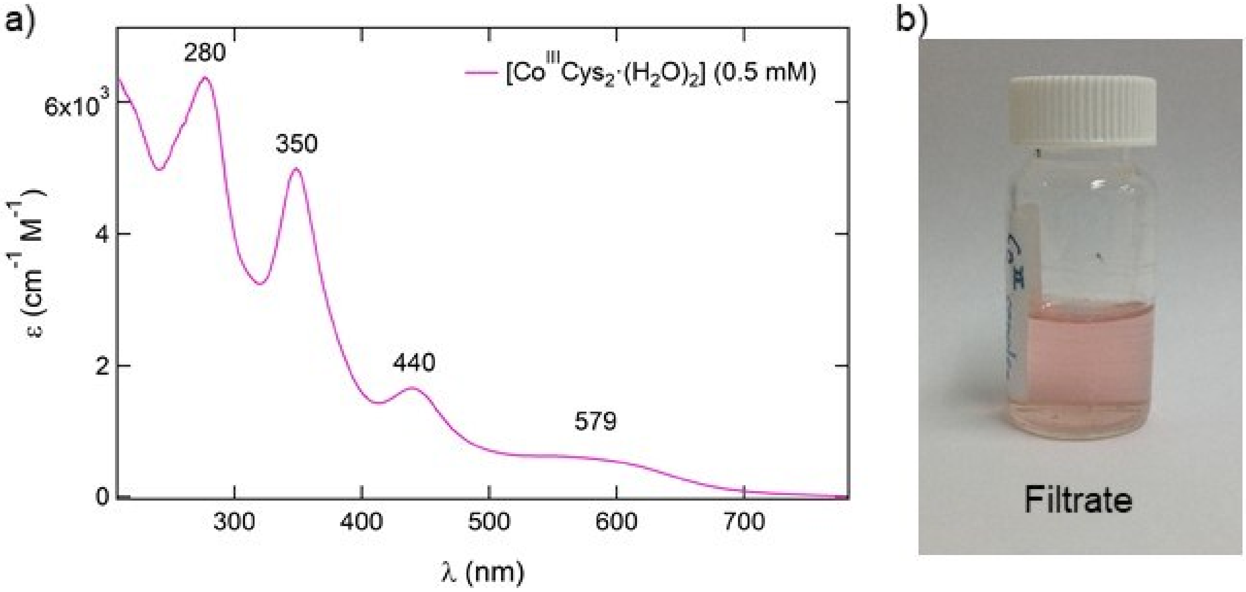

Figure S11. a) UV-vis absorbance spectrum of the isolated Co^{III} bis-cysteinate complex in aqueous solution. b) Filtrate collected after isolating the Co^{III} bis-cysteinate from solution.

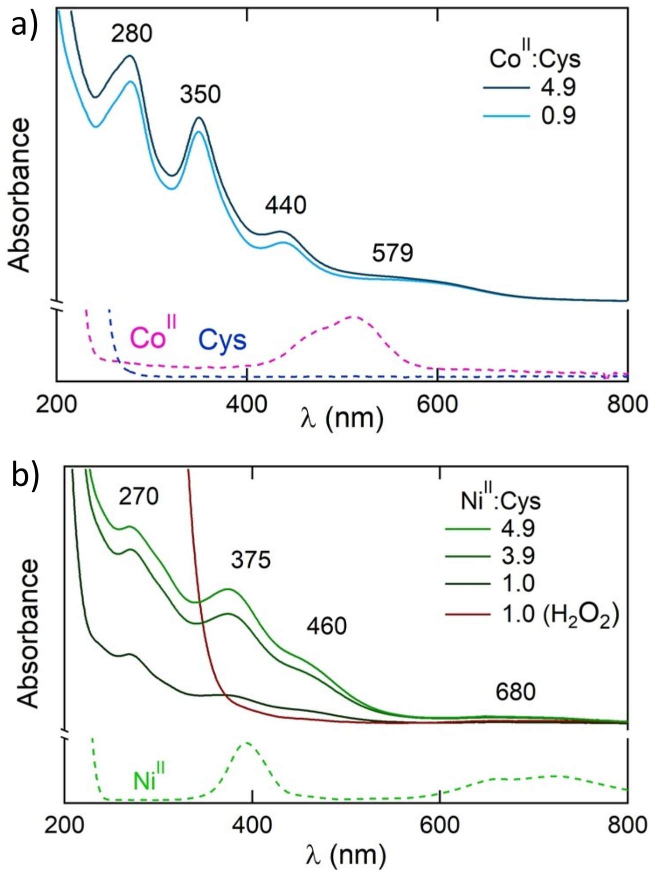

Figure S12. a) UV-vis absorbance spectra for Co^{II}:Cys = 0.9 and 4.9 mole ratio solutions compared to reference for Co^{II} acetate and cysteine aqueous solutions (4.3 mM and 8.8 mM respectively). b) UV-vis absorbance spectra for Ni^{II}:Cys = 1.0, 3.9 and 4.9 mole ratio solutions including aqueous Ni^{II} acetate (40.2 mM).

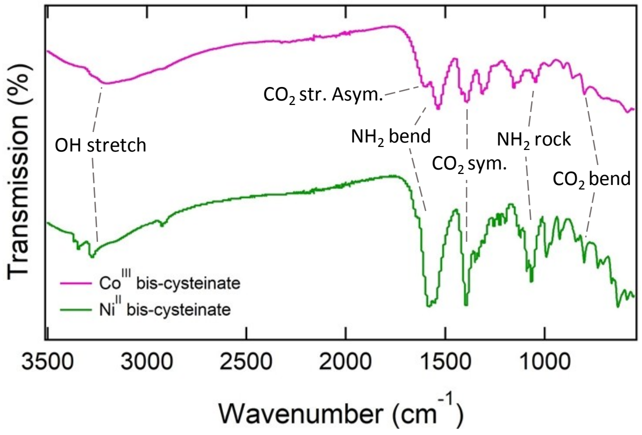

Figure S13. FTIR spectrum of isolated Co^{III} bis-cysteinate (pink) and Ni^{II} bis-cysteinate (green).

By mixing a cobalt(II) acetate (67 mM) aqueous solution into a constantly degassing aqueous solution of cysteine (21 mM) the change in solution colour upon exposure to atmosphere is demonstrated. Both cobalt(II) acetate and cysteine had been degassed prior to mixing by bubbling N_2 for 30 minutes. The colour change is shown in Figure S15. Immediately after mixing the solution colour was orange/red (Figure S15a) then through continued exposure to atmosphere the solution colour turned to dark green/brown (Figure S15c). Studies on the oxidation of cobalt-cysteine complexes have reported a similar colour change on exposure to atmosphere.[9-11]

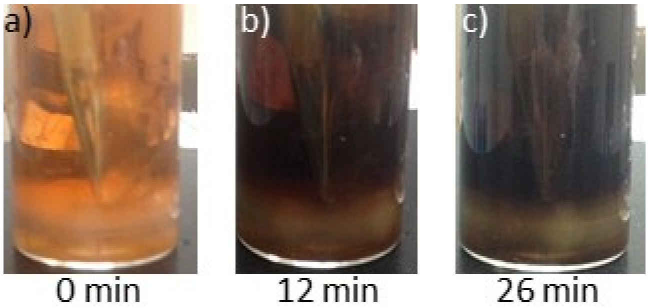

Figure S14. Optical images of the colour change of a 4.85 Co^{II}:Cys solution under constant degassing by bubbling of N_2. a) Image taken immediately after the Co^{II} acetate solution was mixed into the cysteine solution, b) 12 minutes after continuous bubbling with N_2 and c) 26 minutes after continuous bubbling.

S8 Ion Chromatographs

The extracted ion chromatographs for m/z = 18, 44 and 64 are shown in Figure S16 for Co^{III} bis-cysteinate and Ni^{II} bis-cysteinate.

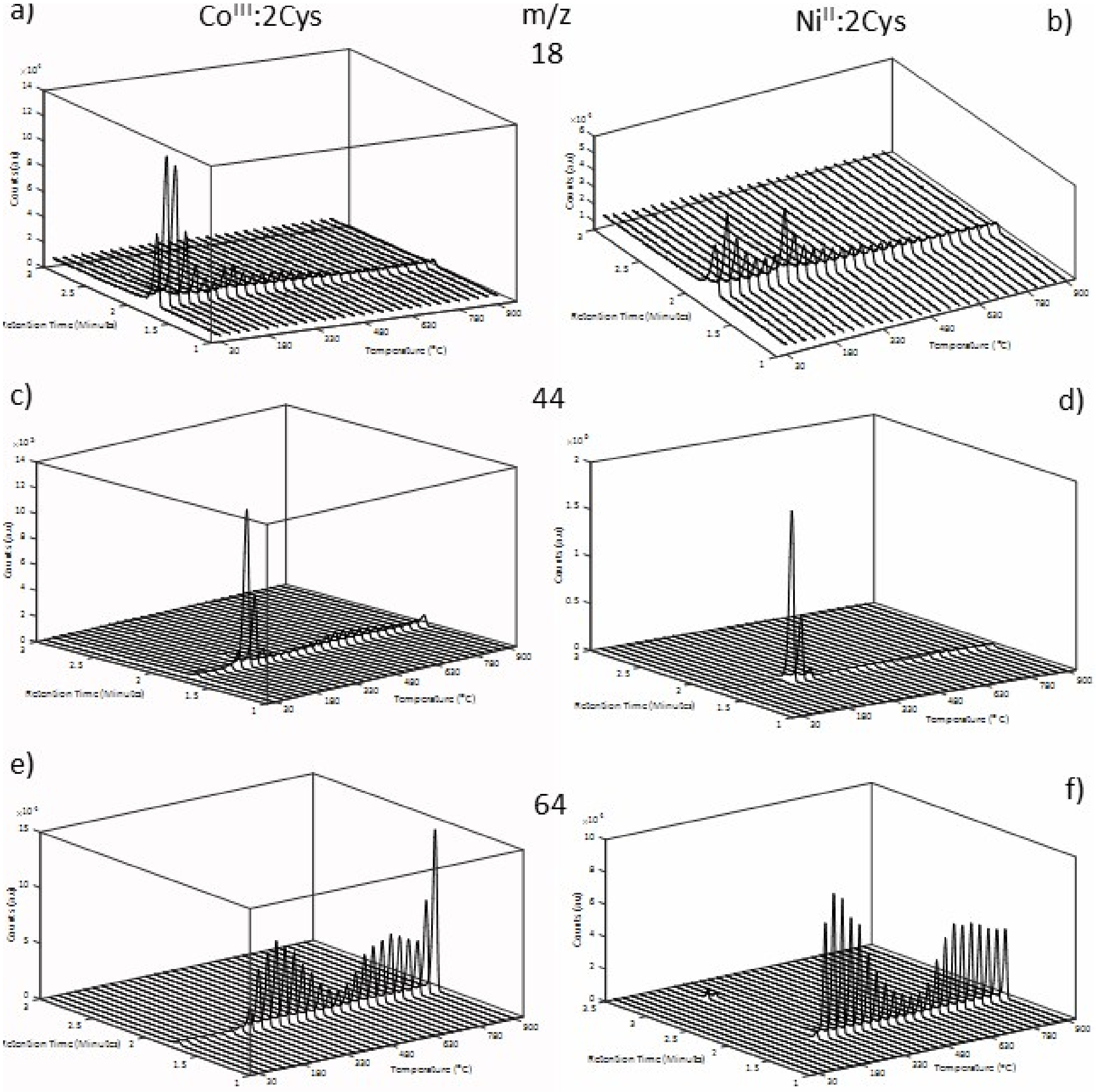

Figure S15. Extracted ion chromatographs for Co^{III} bis-cysteinate and Ni^{II} bis-cysteinate for m/z =18 (a and b), m/z =44 (c and d) and m/z =64 (e and f).

S9 pXRD of TGA-GC-MS residue

Powder X-ray diffraction data for the Co^{III} bis-cysteinate TGA-GC-MS residue after heated to 900°C is shown in Figure S17. The peak intensities were in good agreement with the cubic Co_9S_8 phase (PDF 04-005-4525).

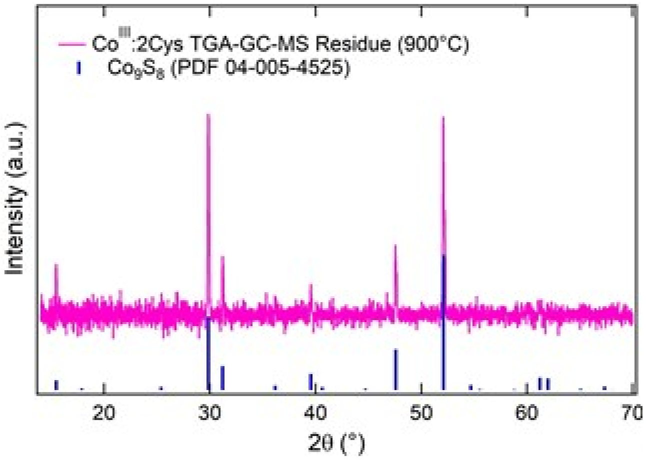

Figure S16. Powder X-ray diffraction pattern of Co^{III} bis-cysteinate TGA-GC-MS residue after heating to 900°C.

Powder X-ray diffraction data for the Ni^{II} bis-cysteinate TG-GC-MS residue after heated to 900°C is shown in Figure S18. The peak intensities were in good agreement with the $Ni_3S_{1.783}$ phase (PDF 04-006-5637).

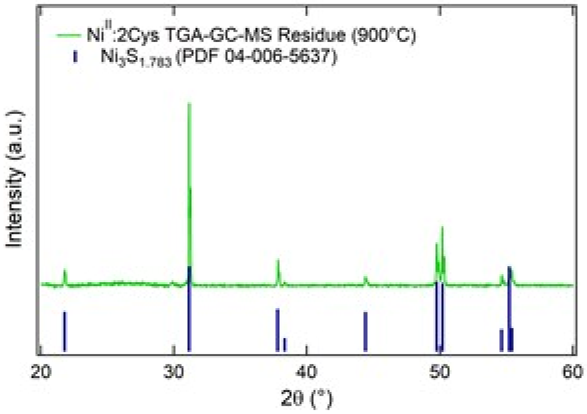

Figure S17. Powder X-ray diffraction pattern of Ni^{II} bis-cysteinate TGA-GC-MS residue after heating to 900°C.

References

1. Ding, Y.; Wang, Z. L., Structure analysis of nanowires and nanobelts by transmission electron microscopy. ACS Publications: 2004.
2. Lever, A. B. P., *Inorganic electronic spectroscopy*. Elsevier: Amsterdam, Netherlands, 1968.
3. Lever, A. B. P., Electronic spectra of dn ions. In *Inorganic electronic spectroscopy*, Elsevier: Amsterdam, Netherlands, 1984; Vol. 2.
4. Dingle, R., Electronic spectrum of crystalline bis (diethyldithiocarbamato) nickel (II). *Inorg. Chem.* **1971,** *10* (6), 1141-1144.
5. Bajia, S. C.; Mishra, A., Synthesis and spectroscopic characterization of bis (N-alkyldithiocarbamato) nickel (II) complexes: crystal structures of [Ni (S2CNH (n-Pr)) 2] and [Ni (S2CNH (i-Pr)) 2]. *J. Coord. Chem.* **2011,** *64* (15), 2727-2734.
6. Angeloski, A.; Baker, A. T.; Bhadbhade, M.; McDonagh, A. M., Bis (κ 2 S, S′-di (isopropyl) dithiocarbamato) nickel (II): Anagostic C–H··· Ni interactions and physical properties. *J. Mol. Struct.* **2016,** *1113*, 127-132.
7. Baidya, N.; Ndreu, D.; Olmstead, M. M.; Mascharak, P. K., Synthesis, structure, and properties of potassium bis (L-cysteinato-N, S) nickelate (II) sesquihydrate. *Inorg. Chem.* **1991,** *30* (10), 2448-2451.
8. Tiedemann, M. T. Heme Binding and Transfer in the Isd Heme Scavenging Pathway of Staphylococcus aureus. The University of Western Ontario, London, ON, 2012.
9. Schubert, M. P., Cobalt complexes of cysteine. *J. Am. Chem. Soc.* **1931,** *53* (10), 3851-3861.
10. Neville, R. G.; Gorin, G., Cysteine Complexes with the Cobalt (III) Ion. I. The Mononucleate Structure of Cobalt (III) Bis-cysteinate. *J. Am. Chem. Soc.* **1956,** *78* (19), 4891-4893.
11. Bresson, C.; Spezia, R.; Esnouf, S.; Solari, P. L.; Coantic, S.; Den Auwer, C., A combined spectroscopic and theoretical approach to investigate structural properties of Co (II)/Co (III) tris-cysteinato complexes in aqueous medium. *New J. Chem.* **2007,** *31* (10), 1789-1797.